Original Research

Modeling of Shakedown Accumulation of Secondary Deformation of Granular Soils Subjected to Low-Amplitude High-Cycle Loading

Pengfei Jia[1], Ruike Li[1], Xiaohui Ren[2], Wenhang Qu[1], Song Yu[3], Yong Wang[4*]

[1]State Key Laboratory of Continental Dynamics Department of Geology Northwest University,
Xi'an, 710069, the People's Republic of China
[2]Shaanxi Expressway Testing & Measuring Co., Ltd., Xi'an 710086, the People's Republic of China
[3]China Railway Major Bridge Reconnaissance & Design Institute Co., Ltd.,
Wuhan 430050, the People's Republic of China
[4]State Key Laboratory of Geomechanics and Geotechnical Engineering Institute of Rock and Soil Mechanics
Chinese Academy of Sciences, Wuhan, 430071, the People's Republic of China

Abstract

The progressive accumulation of secondary deformation, occurring incrementally under low-amplitude, high-cycle loading in soils, can lead to significant displacement of foundations. This study has developed a novel phenomenological model to describe the shakedown accumulation behavior of secondary deformation in granular soils subjected to low-amplitude, high-cycle loading. Firstly, gradual densification of granular packing yields an average volume strain that obeys a logarithmic law as the cyclic loading persists. A log-hyperbolic function, constrained by a limit, is reasonable, considering that the strain will reach a steady state of finite value as the cycle number approaches infinity. Secondly, cyclic loadings with average stress induce the accumulation of strain in the direction of average stress as the cycle number increases. This has been incorporated into the well-known modified Cam-clay model. Lastly, the proposed model has been calibrated using data obtained from undrained and drained cyclic triaxial tests conducted on uniformly fine-grained sands. The results suggest that the model effectively exhibits important features of the accumulation of both volumetric and deviatoric deformation induced by drained cyclic loading over a large number of cycles.

Keywords: accumulation of secondary deformation, accumulation model, low-amplitude, high-cycle, granular soils

*e-mail: wangyong@whrsm.ac.cn
Tel: (+86)13517246178

Introduction

In recent years, with the rapid development of express rail traffic construction activities such as high-speed railways, inner-city railways, and city underground railways, the issue of ground vibrations generated by high-speed trains has become an increasingly prominent concern. In addition to causing inconvenience to residents, the increasing dynamic impacts resulting from ground vibrations can lead to additional settlements or differential settlements of foundations in the railway tracks and nearby structures. Furthermore, these settlements can accelerate the fatigue of structures. Therefore, a more comprehensive understanding of soil mechanisms during dynamic long-term impacts under high-speed moving loads is indispensable for predicting long-term settlements and the deterioration of railway tracks (see Fig. 1).

High-speed traffic loading is typically characterized by low-amplitude and high-cycle loading with a large number of cycles ($N>10^3$), but with a relatively small dynamic stress amplitude (σ_{am}) in comparison to the average stress state (σ_m) (see Fig. 2a). Under low-amplitude, high-cycle loading, the strength and stiffness of the soil are frequently augmented under drainage conditions. This occurs when the average stress ratio is not exceedingly high, and the cyclic stress amplitude is relatively small (i.e., the cyclic stress path is lower than the failure line), resulting in the soil being densely compressed. Therefore, for a foundation subjected to low-amplitude, high-cycle loading, the settlement arising from the accumulation of secondary deformation in soils under periodic stress-controlled conditions could be an important problem (see Fig. 2b). The secondary deformation, caused by the small dynamic stress amplitude, is distinguishable from the post-compaction deformation that is induced by the average stress state (see Fig. 2c). The so-called accumulation of secondary deformation is that while individual or a few dynamic events may not produce visible deformation, a residual deformation in the structure foundation becomes observable in numerous cases after a large number of cycles. In recent years, numerous drained and undrained high-cycle element tests have been documented in several published works. Experimental findings have revealed that even for low-amplitude cycles, a progressive accumulation of deformation occurs with a large number of cycles [1-4].

The modeling of soil's cyclic loading behavior has been a crucial focal point in the advancement of sophisticated constitutive models [5]. In general, the response of soils to cyclic loading is intricately linked to a multitude of underlying factors (e.g., grain distribution, stress, void ratio, etc.) that significantly influence their state [6]. Elastoplastic hysteretic models, such as bounding surface models, delineate each hysteresis loop by employing numerous stress and strain increments, with residual strains resulting from the incomplete closure of stress-strain hysteresis loops [7,

8]. Nevertheless, the practical utility of these models is constrained by the cumulative effect of systematic errors over a large number of cycles, leading to potentially unreliable computations in extensive applications [9]. Empirical accumulation models are primarily constructed through the fitting of experimental data derived from cyclic element tests. The constitutive relationships are commonly represented by closed-form solutions or differential equations, often within the confines of particular boundaries and loading conditions [10-12]. Nevertheless, these models present practical solutions to engineering challenges, given that the boundary conditions correspond to those of laboratory experiments. The empirical function is widely applied in practice owing to its comparatively straightforward mathematical formulation and minimal parameters. Moreover, it serves as a foundation for the development of more sophisticated constitutive models.

In the early literature, various empirical functions have been developed for predicting accumulated deformation in soil under cyclic loading. Many of these functions use a power law relationship between accumulated deformation and the number of load cycles [13]. Another class of empirical functions uses logarithmic formulations to describe the evolution of strain accumulation in relation to the number of cycles [14]. The development of more mechanical and less empirical models for predicting the accumulation behavior of plastic deformation of soils under cyclic loading has become a subject of increasing interest [15-25]. Niemunis et al. formulated a high-cycle accumulation model for granular materials, widely recognized as the Bochum accumulation model [16]. In contrast to previous empirical models, they utilized a tensorial formulation, considering factors such as the number of cycles, void ratio, strain amplitude, mean hydrostatic pressure, and mean stress ratio, among others. The Bochum model relies on numerous parameters established through comprehensive laboratory testing [9]. Despite its tensorial approach, the evolution of accumulated strain in the Bochum model seems to retain an empirical nature, and integrating this model into a cohesive finite element framework poses challenges [17, 18]. Suiker proposed an alternative approach to modeling the long-term behavior of granular materials [15]. This method delineates long-term cyclic densification using a shakedown concept, assuming that no plastic deformation occurs if the cyclic load magnitude remains below the elastic limit. Upon surpassing this threshold, plastic deformation gradually decreases or increases, known as shakedown and non-shakedown, respectively. Suiker's cyclic densification model exhibits similarities to the well-established Perzyna viscoplastic model [26], employing an "overstress formulation" to portray permanent deformation generated per cycle. The model proposes that permanent deformation arises from two distinct mechanisms: frictional sliding and volumetric compaction. One drawback of Suiker's model is the absence of consideration for dilatancy characteristics.
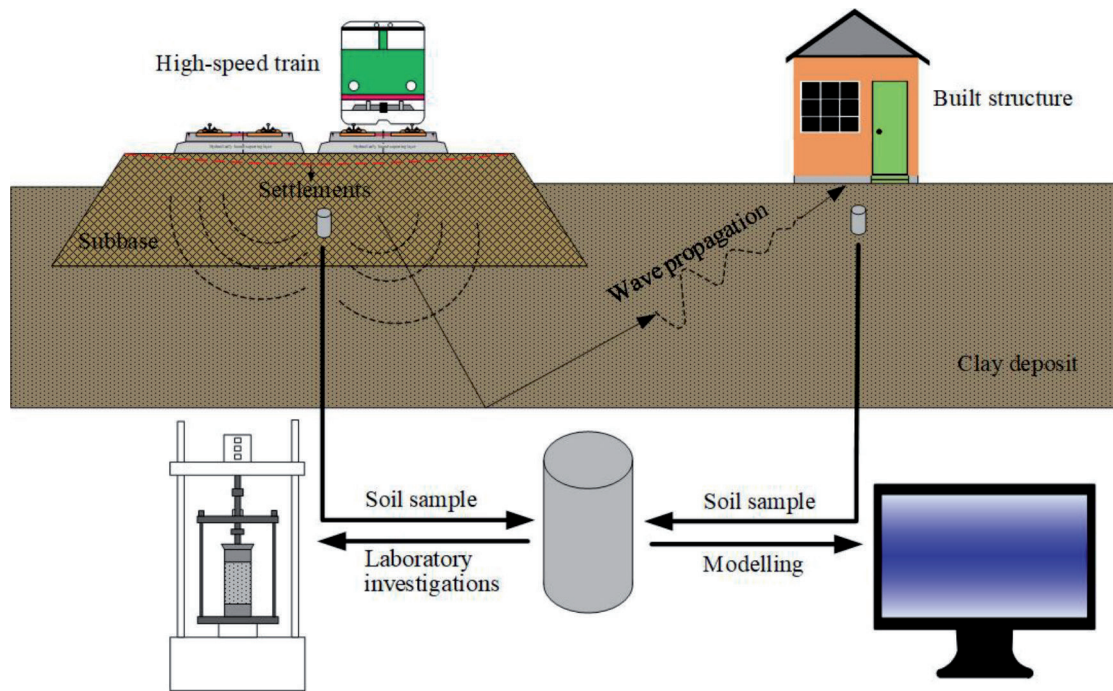
Fig. 1. Ground vibrations cause the differential and additional settlements of the railway track and structure foundations built nearby during the dynamic long-term impacts under the high-speed moving loading.

Recently, Chen et al. proposed a method to determine the plastic shakedown limit of granular materials subjected to cyclic loading based on shakedown theory. This method used a logarithmic function with a defined limit for characterizing the shakedown ranges of the accumulated axial strain, which can be divided into the post-compaction compression part and the secondary cyclic compression part [19].

While several models have been proposed to evaluate the permanent strain accumulation of soils under cyclic loading, it is worth noting that these models are generally one-dimensional. The objective of the current paper is to develop a three-dimensional accumulation model for granular soils subjected to low-amplitude, high-cyclic loading, incorporating the void ratio as a state parameter. An empirical law employing a logarithmic function with a defined limit is utilized to describe the volumetric compaction during the process of cyclic densification when soils experience both isotropic and deviatoric stress variations. Moreover, cyclic triaxial tests have demonstrated that the direction of strain accumulation due to high-cyclic loading mainly depends on the average stress ratio, with minimal influence from the average mean pressure, strain loop characteristics (span, shape, polarization), void ratio, loading frequency, static preloading, and grain size distribution curve [9]. The proposed model employs a unique flow rule based on the modified Cam-clay model, which only depends on the average stress ratio to describe the direction of accumulation of secondary deformation. A more detailed discussion is given in Section 2.

The structure of this paper is as follows: Section 2 presents the overarching approach and formulates the accumulation model based on triaxial and general stress states. In Section 3, the accumulation model is calibrated and validated utilizing data from cyclic triaxial tests conducted on sands.

Methodologies

Strain Decomposition

For a state variable caused by non-monotonic loads, we can define its average value $\sqcup_m$ to be the center of the smallest hypersphere that encompasses all states $\sqcup$ upon the cycle. The amplitude of a state variable is defined as $\sqcup_{am} = \max|\sqcup - \sqcup_m|$ (see Fig. 2a). The effective Cauchy stress tensor is decomposed as:

$$\boldsymbol{\sigma}' = \boldsymbol{\sigma}'_m + \boldsymbol{\sigma}_{am} \qquad (1)$$

Where σ'_m is the average (static) component of the stress tensor and σ_{am} is the amplitude cyclic component of the stress tensor. It is assumed that the cyclic component is relatively small compared to the average component, which reflects the fact that the stress conditions in the soil beneath a structure subjected to high-cyclic dynamic loading impacts. The strain tensor is similarly decomposed as:

$$\boldsymbol{\varepsilon} = \boldsymbol{\varepsilon}_m + \boldsymbol{\varepsilon}_{am} \qquad (2)$$

where The cyclic component of the strain tensor undergoes short-term variations due to the low-amplitude cyclic component of the stress tensor and
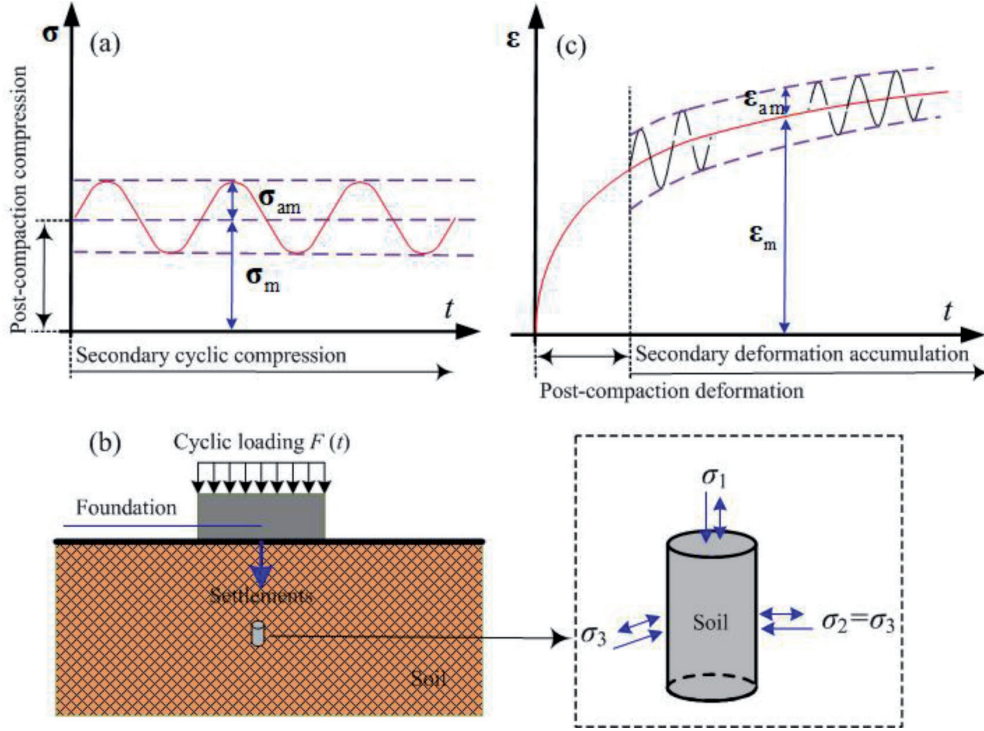
Fig. 2. Accumulation of secondary deformation proceeding cycle by cycle under stress-controlled conditions: stress cycles leave strain accumulation.

is controlled by the elastic behavior of the material. Under stress-controlled, fully drained conditions, as a result, the stress loops are closed and the material reacts with not perfectly closed strain loops, and thus the strain accumulates. The average part of the strain tensor gradually increases as the cycle number increases (see Fig. 2c). In the following subsections, a new accumulation model will be derived that captures only the average response of the stress-strain behavior under cyclic loading, reflecting the accumulation of secondary deformation proceeding cycle by cycle.

As a start, compression stress and compression strain are used as positive values, whereas tensile stress and tensile strain are negative. The average strain rate $\dot{\varepsilon}_m$ is separated into an elastic (recoverable) strain rate $\dot{\varepsilon}_m^e$ and an inelastic (irrecoverable) strain rate $\dot{\varepsilon}_m^i$ as:

$$\dot{\boldsymbol{\varepsilon}}_m = \dot{\boldsymbol{\varepsilon}}_m^e + \dot{\boldsymbol{\varepsilon}}_m^i = \dot{\boldsymbol{\varepsilon}}_m^e + \dot{\boldsymbol{\varepsilon}}_m^p + \dot{\boldsymbol{\varepsilon}}_m^{acc} \qquad (3)$$

Where the general term of inelastic strain rate is decomposed into plastic and the accumulated strain rate is denoted by superscripts p and acc, respectively. Note that by separating plastic and accumulated strain rate, we are emphasizing rate independent (for stress paths touching the yield surface) and rate dependent cyclic plasticity, respectively. In the context of cyclic loading, "rate" means a derivative with respect to the number of cycles N, i.e., $\sqcup = d\sqcup/dN$ instead of $\sqcup = d\sqcup/dt$, in which the accumulation of secondary deformations over a number of load cycles N can be regarded as a continuous process (pseudo-creep), and the discrete

number of load cycles N is treated as a "smoothed" continuous time-like variable. For the sake of simplicity, we neglect the plastic strain rate caused by the harmonic loading in this study, then:

$$\dot{\boldsymbol{\varepsilon}}_m = \dot{\boldsymbol{\varepsilon}}_m^e + \dot{\boldsymbol{\varepsilon}}_m^{acc} \qquad (4)$$

A separate elastic relationship is suggested to relate the elastic strain rate $\dot{\varepsilon}_m^e$ in Eq. (4) to the average stress rate σ'_m as:

$$\dot{\boldsymbol{\sigma}}'_m = \mathbf{E} : \dot{\boldsymbol{\varepsilon}}_m^e \qquad (5)$$

where $\mathbf{E}$ is a fourth-order elastic stiffness tensor.

An accumulated strain rate $\dot{\varepsilon}_m^{acc}$ in Eq. (4) is calculated from a flow rule that was originally proposed by Perzyna [26] as:

$$\dot{\boldsymbol{\varepsilon}}_m^{acc} = \gamma \left\langle \varphi(f) \right\rangle \frac{\partial g}{\partial \boldsymbol{\sigma}'_m} = S \frac{\partial g}{\partial \boldsymbol{\sigma}'_m} \qquad (6)$$

Where γ is referred to as the fluidity parameter, φ is an overstress function of the yield function f, and g is a plastic potential function. In our model, a scaling function S is used instead of $\gamma\langle\varphi(f)\rangle$, which will be calculated by means of accumulated volumetric strain. $\partial g/\partial\boldsymbol{\sigma}'_m$ denotes the direction of strain accumulation. The presented results of cyclic triaxial tests on sands demonstrate that the direction of strain accumulation depends essentially on the average stress ratio, while

ACCEPTED MANUSCRIPT

a slight influence of the stress loop (span, shape, polarization), the void ratio, the loading frequency, the static preloading, and the grain size distribution curve is observed when the cycles are performed [6]. These experimental findings prove that the cyclic flow rule can be well approximated by the flow rules of constitutive models for monotonic loading. Therefore, the direction of strain accumulation can be treated separately from the scale function *S* in Eq. (6).

Volumetric Compaction Relationship for 1D Stressing

Yin first introduced a logarithmic hyperbolic function to describe the long-term creep characteristics of clay [27]. In this study, we suggest a similar logarithmic hyperbolic function with limited accumulated deformation for fitting the nonlinear accumulation behavior of granular soils under high-cyclic loading. It is expressed as:

$$\varepsilon_{vm}^{acc} = \frac{\psi \ln(1+N)}{1 + \dfrac{\psi}{\varepsilon_{vml}^{acc}} \ln(1+N)} \tag{7}$$

where ψ and ε_{vml}^{acc} are two constant parameters. ε_{vml}^{acc} is the limit accumulated strain, and ψ is a fitting parameter. From Eq. (7), it is also found that when $N = \infty$, $\varepsilon_{vm}^{acc} = \varepsilon_{vml}^{acc}$. This implies that there is a limit for the accumulated volume strain. With the increase of the cycle number, the volume strain due to accumulation will never exceed this volume strain limit of ε_{vml}^{acc}. That is to say, after a specific number of load cycles, the material response turns into a shakedown. However, this function is generally reasonable, as the utilization of granular locking during the process of progressive material compaction serves to prevent the unlimited expansion of the associated accumulated deformation.

Differentiating Eq. (7) leads to the accumulation rate with respect to *N*:

$$\dot{\varepsilon}_{vm}^{acc} = \frac{\psi}{1+N} \frac{1}{\left(1 + \dfrac{\psi}{\varepsilon_{vml}^{acc}} \ln(1+N)\right)^2} \tag{8}$$

This is the so-called "time" hardening formulation. Another formulation can be obtained by eliminating time (the number of cycles) from Eq. (7). This brings in the strain and leads to the so-called strain hardening formulation, in which the accumulation rate in a variable stress situation depends on the stress (through the parameters that will be discussed in the next section). In this method, Eq. (8) is written as:

$$\dot{\varepsilon}_{vm}^{acc} = \psi \left(1 - \frac{\varepsilon_{vm}^{acc}}{\varepsilon_{vml}^{acc}}\right)^2 \exp\left(\frac{1}{\psi \varepsilon_{vml}^{acc}} \left(1 - \frac{\varepsilon_{vml}^{acc}}{\varepsilon_{vm}^{acc}}\right)\right) \tag{9}$$

Three-Dimensional Generalization

In this study, an associated plastic flow rule is employed, where the plastic potential function *g* in Equation (6) is equivalent to the flow-surface function *f*, which depends on stress level and hardening history. Based on the results of drained cyclic triaxial tests, the flow rule of the modified Cam-clay model can well approximate the measured $\dot{\varepsilon}_{vm}^{acc}/\dot{\varepsilon}_{qm}^{acc}$ ratios [16]. We consider an elliptical plastic potential like that used in the modified Cam-clay model:

$$g = f = p_m'^2 - p_m' p_{m0}' + \frac{q_m^2}{M^2} = 0 \tag{10}$$

where *M* is the slope of the critical state line in the *p-q* space and controls the shape of the plastic potential. $M = M_c = 6\sin\varphi/(3-\sin\varphi)$ in compression, and $M = M_e = 6\sin\varphi/(3+\sin\varphi)$ in extension; φ is the internal friction angle. The value of p_{m0} is the hydrostatic pressure where an elliptical locus meets the *p* axis. If a stress state is known, p_{m0} can be found from Eq. (10):

$$p_{m0}' = p_m' + \frac{q_m^2}{p_m M^2} \tag{11}$$

According to Eq. (6), the accumulated volumetric and deviatoric strain rates, $\dot{\varepsilon}_{vm}$ and $\dot{\varepsilon}_{qm}^{acc}$, respectively, are related to the normal plastic potential at the current stress state as:

$$\dot{\varepsilon}_{vm}^{acc} = S \frac{\partial g}{\partial p_m'} \tag{12}$$

$$\dot{\varepsilon}_{qm}^{acc} = S \frac{\partial g}{\partial q_m} \tag{13}$$

The scaling function *S* can be calculated by Eqs. (9) and (12) as:

$$S = \psi \left(1 - \frac{\varepsilon_{vm}^{acc}}{\varepsilon_{vml}^{acc}}\right)^2 \exp\left(\frac{1}{\psi \varepsilon_{vml}^{acc}} \left(1 - \frac{\varepsilon_{vml}^{acc}}{\varepsilon_{vm}^{acc}}\right)\right) \frac{1}{|\partial g/\partial p_m'|} \tag{14}$$

The general expression for the accumulated strain rates is given by:

$$\dot{\varepsilon}_m^{acc} = \psi \left(1 - \frac{\varepsilon_{vm}^{acc}}{\varepsilon_{vml}^{acc}}\right)^2 \exp\left(\frac{1}{\psi \varepsilon_{vml}^{acc}} \left(1 - \frac{\varepsilon_{vml}^{acc}}{\varepsilon_{vm}^{acc}}\right)\right) \frac{1}{|\partial g/\partial p_m'|} \frac{\partial g}{\partial \sigma_m'} \tag{15}$$

via Eqs. (6) and (14). The description of the model is now complete, and the accumulation model can be summarized as:

$$\dot{\boldsymbol{\sigma}}'_{\mathrm{m}} = \mathbf{E} : \left(\dot{\boldsymbol{\varepsilon}}_{\mathrm{m}} - \dot{\boldsymbol{\varepsilon}}_{\mathrm{m}}^{\mathrm{acc}} \right) \qquad (16)$$

where the accumulation rates $\dot{\boldsymbol{\varepsilon}}_{\mathrm{m}}^{\mathrm{acc}}$ are calculated from Eq. (15).

The components of the accumulation rates contributing to volumetric and deviatoric strains are generated by the first and second terms, respectively, of the differential form of the plastic potential. For the elliptical plastical potential function in Eq. (6), these forms are:

$$\frac{\partial g}{\partial \boldsymbol{\sigma}'_{\mathrm{m}}} = \frac{\partial g}{\partial p'_{\mathrm{m}}} \frac{\partial p'_{\mathrm{m}}}{\partial \boldsymbol{\sigma}'_{\mathrm{m}}} + \frac{\partial g}{\partial q_{\mathrm{m}}} \frac{\partial q_{\mathrm{m}}}{\partial \boldsymbol{\sigma}'_{\mathrm{m}}} \qquad (17)$$

The derivatives of the stress invariants are:

$$\frac{\partial p_{\mathrm{m}}}{\partial \boldsymbol{\sigma}'_{\mathrm{m}}} = \frac{1}{3} \boldsymbol{\delta} \qquad (18)$$

$$\frac{\partial q_{\mathrm{m}}}{\partial \boldsymbol{\sigma}'_{\mathrm{m}}} = \frac{3}{2 q_{\mathrm{m}}} \left(\boldsymbol{\sigma}'_{\mathrm{m}} - p'_{\mathrm{m}} \boldsymbol{\delta} \right) \qquad (19)$$

and the direction of strain accumulation is obtained from:

$$\frac{\partial g}{\partial p'_{\mathrm{m}}} = 2 p'_{\mathrm{m}} - p'_{\mathrm{m}0} \qquad (20)$$

$$\frac{\partial g}{\partial q_{\mathrm{m}}} = \frac{2 q_{\mathrm{m}}}{M^2} \qquad (21)$$

Model Evaluation and Discussion

Cyclic Triaxial Tests

The verification of the proposed model will be performed by employing the cyclic triaxial test data. The tests are done on freshly dense fine sand (ρ_s = 2.63 g/cm³, e_{min} = 0.624, e_{max} = 0.925, d_{50} = 0.23 mm, $U = d_{60}/d_{10}$ = 1.85, φ_c = 33.2). The stress conditions for the axisymmetric specimen have been schematized in Fig. 3. Under triaxial conditions, the soil sample is confined by a hydrostatic stress σ_c, while an additional vertical stress σ_v is applied. The vertical stress is composed of a static part σ_{stat} and a cyclic part σ_{cyc}, which is characterized by a periodic sinusoidal vibration with an amplitude σ_{am} and a frequency f. Apparently, the principal stress, σ_1, results from the summation of the confining pressure σ_c and the vertically applied stress, σ_v, while the principal stress σ_3, is equal to the confining pressure. The stress state is characterized by an average part with the hydrostatic pressure $p_{\mathrm{m}} = \sigma_c + \sigma_{\mathrm{sat}}/3$, the deviatoric stress $q_{\mathrm{m}} = \sigma_{\mathrm{sat}}$, a cyclic part with the amplitude of the hydrostatic pressure $p_{\mathrm{am}} = \sigma_{\mathrm{am}}/3$, and the amplitude of the deviatoric stress $q_{\mathrm{am}} = \sigma_{\mathrm{am}}$ (see Fig. 3). The cyclic stress ratio,

$$\zeta_{\mathrm{am}} = \frac{q_{\mathrm{am}}}{p_{\mathrm{m}}} = \frac{\sigma_{\mathrm{am}}}{p_{\mathrm{m}}} \qquad (22)$$

is used. An axial deformation ε_1 and a radial deformation ε_3 are observed, whereas the strain invariants reduce to:
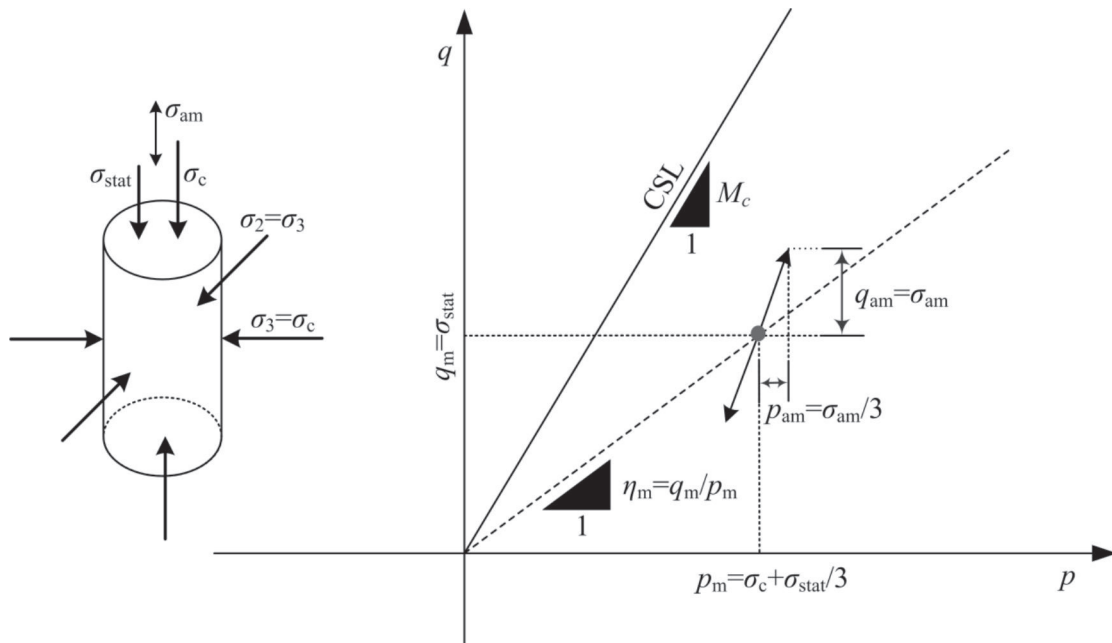

Fig. 3. Stress state in *p-q* space for a cyclic triaxial test: An average stress (described by p_{m} and q_{m}) is superposed by a cyclic portion (described by p_{am} and q_{am}).

ACCEPTED MANUSCRIPT

$$\varepsilon_{\mathrm{v}} = \varepsilon_1 + 2\varepsilon_3 \tag{23}$$

$$\varepsilon_{\mathrm{q}} = \frac{2}{3}\left|\varepsilon_1 - \varepsilon_3\right| \tag{24}$$

Determination of the Elastic Stiffness E

The elastic stiffness **E** interrelates the trends of stress and strain evolution in Eq. (16). If the elastic deformation of the soil is assumed to be isotropic, there are only two constants (or modules) as:

$$\mathbf{E} = \frac{3K}{1+\nu}\left((1-2\nu)\mathbf{I} + \nu\,\boldsymbol{\delta}\otimes\boldsymbol{\delta}\right) \tag{25}$$

Where **I** is a fourth-order identity tensor which is defined as $I_{ijkl}=(1/2)(\delta_{ik}\delta_{jl}+\delta_{il}\delta_{jk})$ and $\boldsymbol{\delta}$ is a second-order Kronecker unit tensor with a Kronecker's symbol δ_{ij}, $\otimes$ denotes tensor product. ν is the Poisson's ratio. The shear modulus G can be deduced as:

$$G = \frac{3(1-2\nu)K}{2(1+\nu)} \tag{26}$$

For an axisymmetric stress state, it is convenient to rewrite eq. (16) with Roscoe's invariants as:

$$\begin{pmatrix} \dot{p}'_{\mathrm{m}} \\ \dot{q}_{\mathrm{m}} \end{pmatrix} = \begin{pmatrix} K & 0 \\ 0 & 3G \end{pmatrix} \begin{pmatrix} \dot{\varepsilon}_{\mathrm{vm}} - \dot{\varepsilon}_{\mathrm{vm}}^{\mathrm{acc}} \\ \dot{\varepsilon}_{\mathrm{qm}} - \dot{\varepsilon}_{\mathrm{qm}}^{\mathrm{acc}} \end{pmatrix} \tag{27}$$

Where K is a bulk modulus and G is a shear modulus. In a drained test with stress-controlled cycles, the ratio of the rates of volumetric and deviatoric portions corresponds to the well-known formula of the modified Cam-clay model as:

$$\frac{\dot{\varepsilon}_{\mathrm{vm}}^{\mathrm{acc}}}{\dot{\varepsilon}_{\mathrm{qm}}^{\mathrm{acc}}} = \frac{M^2 - \eta_{\mathrm{m}}^2}{2\eta_{\mathrm{m}}} \tag{28}$$

For a stress-controlled isotropic stress state, $q_{\mathrm{m}} = 0$, $\dot{q}_{\mathrm{m}} = 0$. Under undrained conditions, $\dot{\varepsilon}_{\mathrm{vm}} = 0$, Eq. (27) takes the form of pore pressure accumulation (isotropic relaxation) as:

$$\dot{u} = K\dot{\varepsilon}_{\mathrm{vm}}^{\mathrm{acc}} \tag{29}$$

Under drained conditions, $\dot{p}'_{\mathrm{m}} = 0$, Eq. (27) takes the form of volumetric strain accumulation as:

$$\dot{\varepsilon}_{\mathrm{vm}} = \dot{\varepsilon}_{\mathrm{vm}}^{\mathrm{acc}} \tag{30}$$

The bulk modulus, K, can be obtained from the ratio of the rate of pore pressure accumulation, $\dot{u}$, in an undrained cyclic triaxial test to the rate of volumetric strain accumulation, $\dot{\varepsilon}_{\mathrm{vm}}^{\mathrm{acc}}$, in a drained cyclic triaxial test with similar initial stress, void ratio, and cyclic loading.

$$K = \frac{\dot{u}}{\dot{\varepsilon}_{\mathrm{vm}}^{\mathrm{acc}}} \tag{31}$$

In combination with a constant Poisson's ratio ν, the shear modulus G can be calculated from Eq. (26).

For evaluation of bulk modulus, $K = \dot{u}/\dot{\varepsilon}_{\mathrm{vm}}^{\mathrm{acc}}$, 12 drained and undrained cyclic triaxial tests (see Table 1) at different stress levels p_{m} and stress ratio η_{m} are carried out. All tests were performed with uniform, medium-coarse to coarse quartz sand. All samples are prepared

Table 1. Stress conditions for the tests used for model calibration.

	p_{m} (kPa)	q_{m} (kPa)	η_{m} (-)	ζ_{am} (-)
Test 1	100	0	0.000	0.300
Test 2	100	50	0.500	0.300
Test 3	100	75	0.750	0.300
Test 4	100	100	1.000	0.300
Test 5	200	0	0.000	0.300
Test 6	200	100	0.500	0.300
Test 7	200	150	0.750	0.300
Test 8	200	200	1.000	0.300
Test 9	300	0	0.000	0.300
Test 10	300	150	0.500	0.300
Test 11	300	225	0.750	0.300
Test 12	300	300	1.000	0.300

ACCEPTED MANUSCRIPT

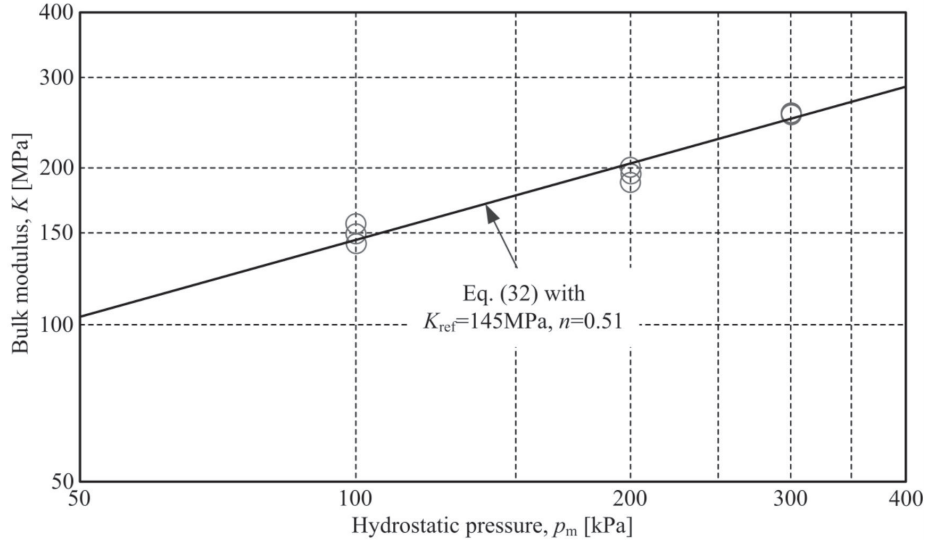Fig. 4. Bulk modulus K determined by the comparison with the data from the cyclic triaxial tests as a function of hydrostatic pressure p_{m}.

with a relative density of about 60%. The mean grain diameter d_{50} is equal to 0.56mm and the maximum void ratio $e_{\max}$ and minimum void ratio $e_{\min}$ are equal to 0.942 and 0.573, respectively. The critical friction angle φ_c is equal to 37.7. For each pair of drained and undrained cyclic tests, the bulk modulus, K, is calculated from Eq. (31). In all tests (drained and undrained), the first cycle may be irregular and may generate much more deformation than subsequent ones. The proposed accumulation model predicts only the accumulation due to the subsequent regular cycles. As for numerical calculations with the proposed accumulation model, we will calculate the first cycle using a conventional implicit constitutive model. So the first cycle is not included in the evaluation of bulk modulus. In all diagrams, $N = 1$ refers to the first regular cycle. The rates $\dot{u}$ and $\dot{\varepsilon}_{\mathrm{vm}}^{\mathrm{acc}}$ are calculated for 20 load cycle increments. Fig. 4 presents the bulk modulus K versus average hydrostatic p_{m}. The obvious pressure-dependence of K can be approximated by:

$$K = K_{\mathrm{ref}} \left(\frac{p_{\mathrm{m}}}{p_{\mathrm{atm}}} \right)^{1-n} \tag{32}$$

With $K_{\mathrm{ref}} = 145$ MPa and $n = 0.51$ (the thick solid line in Fig. 4). The p_{atm} is the standard atmospheric pressure, i.e., $p_{\mathrm{atm}} = 100$ kPa. Furthermore, a constant Poisson's ratio $v = 0.3$ is assumed, which is appropriate for medium density compacted sands.

Determination of the Accumulation Model Parameters $\varepsilon_{\mathrm{vml}}^{\mathrm{acc}}$, Ψ

As mentioned above, $\varepsilon_{\mathrm{vml}}^{\mathrm{acc}}$ is the limit of volume strain accumulation in Eq. (7). The determination of $\varepsilon_{\mathrm{vml}}^{\mathrm{acc}}$ is not an easy task because it is impossible to run a test of an infinite cycle. However, $\varepsilon_{\mathrm{vml}}^{\mathrm{acc}}$ will have an upper bound value. In an extreme case, assuming the void ratio of a soil element (or specimen) all becomes the minimum void ratio $e_{\min}$ under accumulation at infinite cycle, the upper bound limit is $\varepsilon_{\mathrm{vml, uper}}^{\mathrm{acc}} = e_{\min}/(1 + e_{\min})$. Since $e_{\min} = 0.573$, the upper limit value of volume strain accumulation $\varepsilon_{\mathrm{vml, uper}}^{\mathrm{acc}} = 1.342$ for medium dense compacted sands in this paper. In case no long-term accumulation data are available, the limit value of volume strain accumulation can be estimated from curve-fitting test data.

For curve fitting and determination of $\varepsilon_{\mathrm{vm}}^{\mathrm{acc}}$ and ψ, Eq. (7) can be written as:

$$\frac{\ln(1+N)}{\varepsilon_{\mathrm{vm}}^{\mathrm{acc}}} = \frac{1}{\varepsilon_{\mathrm{vml}}^{\mathrm{acc}}} \ln(1+N) + \frac{1}{\psi} \tag{33}$$

The measured data of volume strain accumulation against the number of cycles is used to calculate the relationship between the normalized ratio $\ln(1+N)/\varepsilon_{\mathrm{vm}}^{\mathrm{acc}}$ and $\ln(1+N)$. For isotropic stress, it is found that the data points of $\ln(1+N)/\varepsilon_{\mathrm{vm}}^{\mathrm{acc}}$ against $\ln(1+N)$ are almost on a straight line (see Fig. 5). Comparing the best-fitting equation with Eq. (33), over a load cycle increment $[N, N + \Delta N]$, $\varepsilon_{\mathrm{vm}}^{\mathrm{acc}}$ and ψ can be computed as:

$$\frac{1}{\varepsilon_{\mathrm{vml}}^{\mathrm{acc}}} = \frac{\dfrac{\ln(1+N+\Delta N)}{\varepsilon_{\mathrm{vm}, N+\Delta N}^{\mathrm{acc}}} - \dfrac{\ln(1+N)}{\varepsilon_{\mathrm{vm}, N}^{\mathrm{acc}}}}{\ln\left(\dfrac{1+N+\Delta N}{1+N}\right)} \tag{34}$$

Table 2. Values of the parameters in eq. (7) or eq. (33) obtained by curve fitting.

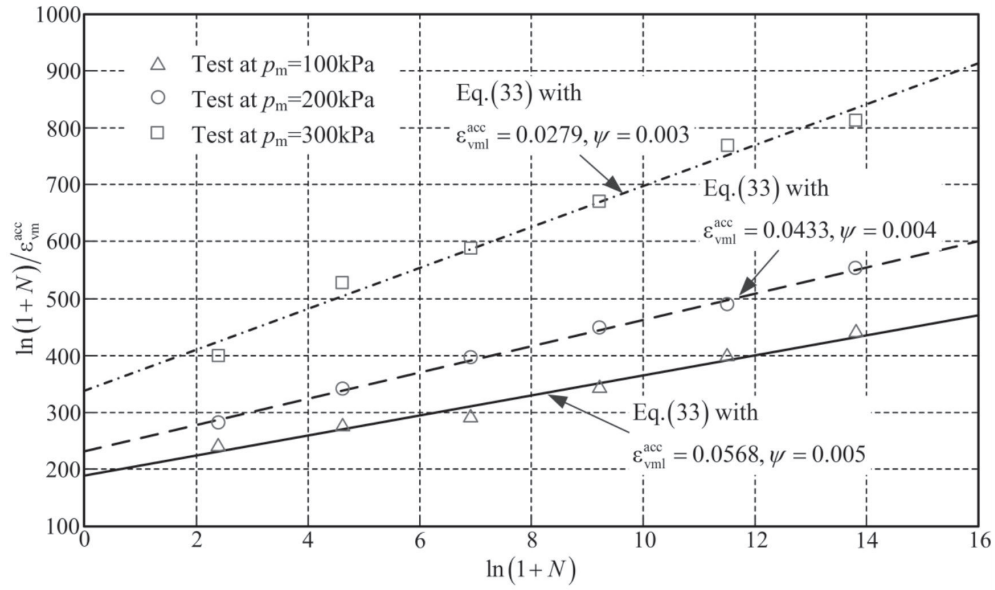| p_{m} (kPa)	100	200	300
$\varepsilon_{\mathrm{vml}}^{\mathrm{acc}}$	0.0568	0.0433	0.0279
Ψ	0.005	0.004	0.003

ACCEPTED MANUSCRIPT

Fig. 5. Comparison of measured data and fitting curve by a straight line obtained from the normalized ratio $\ln(1 + N)/\varepsilon_{vm}^{acc}$ to $\ln(1+N)$ for tests at $p_m = 100$ kPa, 200 kPa, 300 kPa respectively.
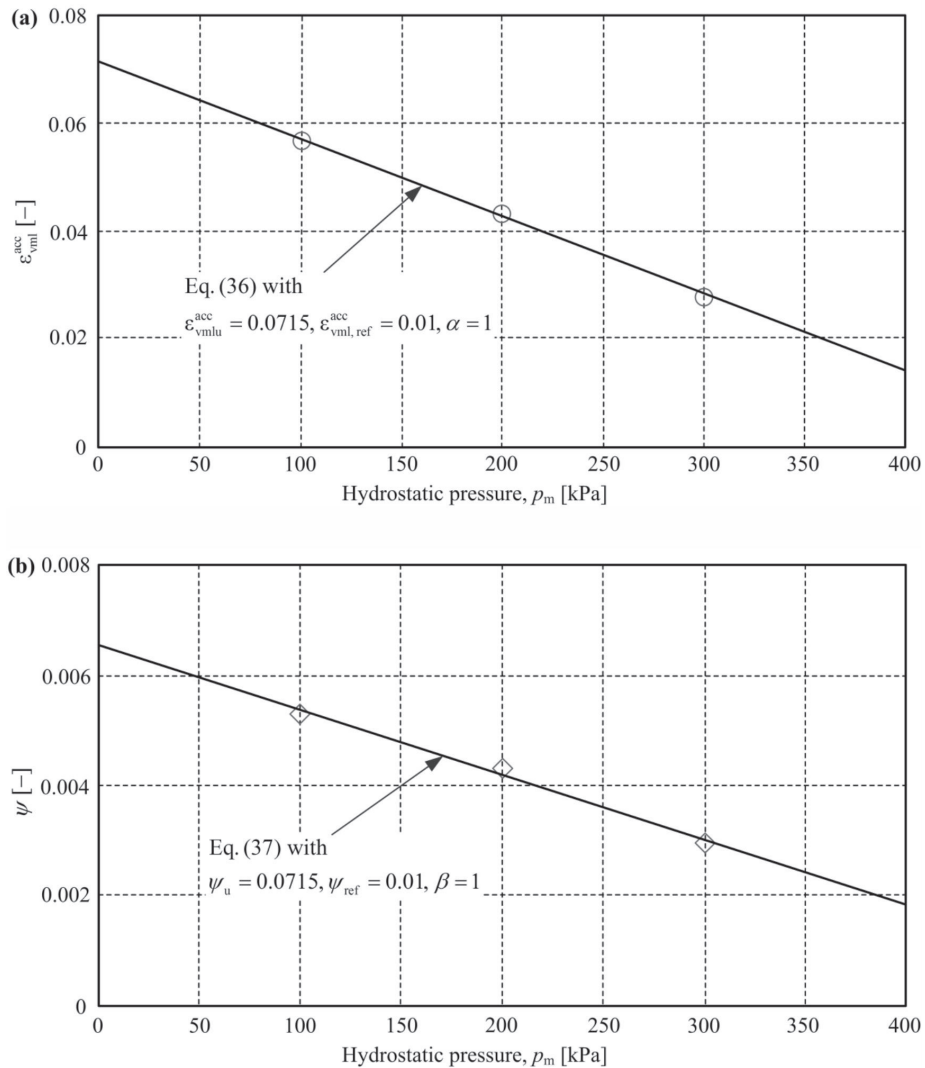

Fig. 6. Relationship of accumulation model paramters a) ε_{vml}^{acc} and b) ψ to the isotropic stress p_m scale on a straight line respectively.
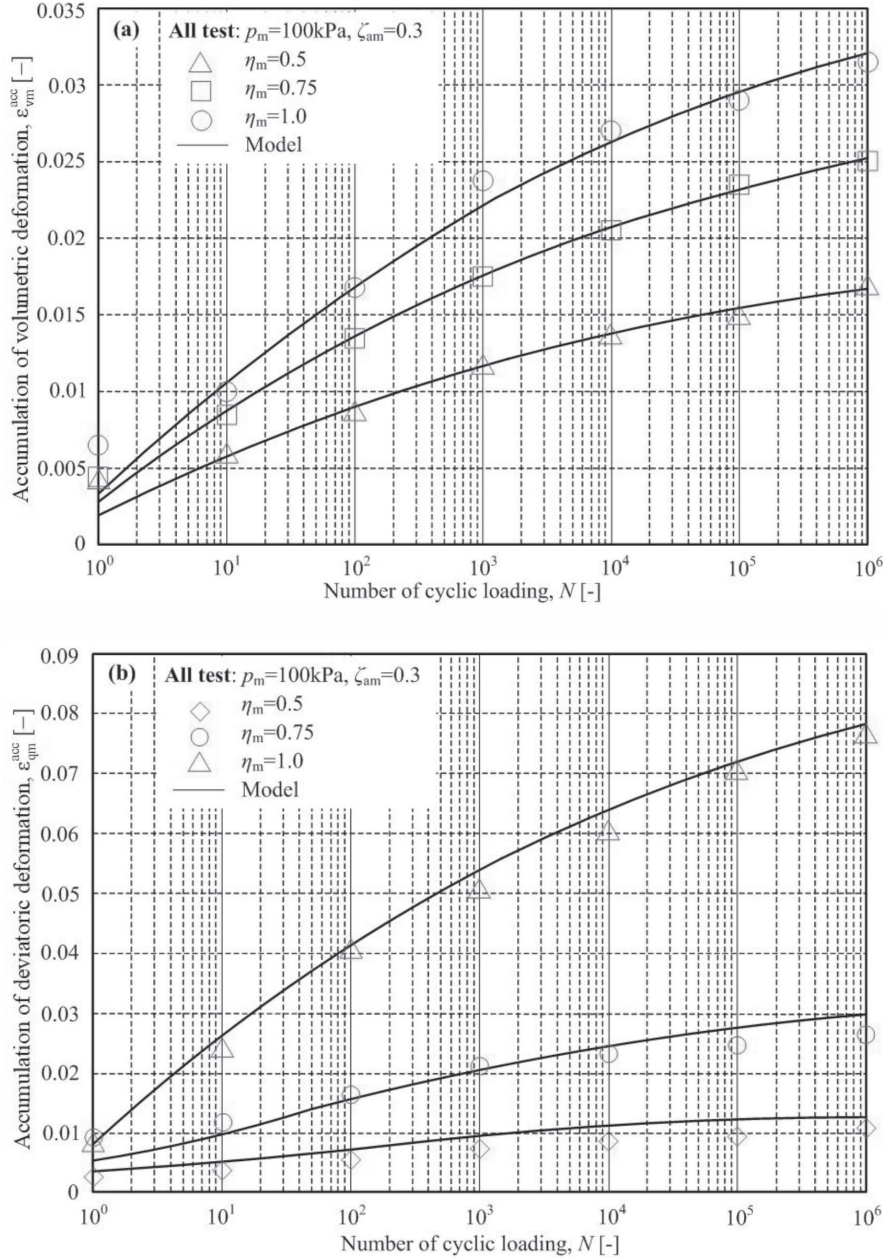
Fig. 7. Experimental results of cyclic triaxial tests versus predictions of model: accumulation of a) volumetric deformation, ε_{vm}^{acc} and (b) deviatoric deformation, ε_{qm}^{acc} over 10^6 cycles under axi-symmetrical stress conditions at hydrostatic pressure $p_m = 100$ kPa, cyclic stress ratio $\zeta_{am} = 0.3$, and avegage stress ratio $\boldsymbol{\eta}_m = 0.5, 0.75, 1.0$ respectively.

and

$$\frac{1}{\psi} = \frac{\ln(1+N)}{\varepsilon_{vm,N}^{acc}} - \frac{\dfrac{\ln(1+N+\Delta N)}{\varepsilon_{vm,N+\Delta N}^{acc}} - \dfrac{\ln(1+N)}{\varepsilon_{vm,N}^{acc}}}{\ln\left(\dfrac{1+N+\Delta N}{1+N}\right)} \ln(1+N)$$

(35)

For isotropic stress of 100 kPa, computing the data points of $\ln(1 + N)/\varepsilon_{vm}^{acc}$ against $\ln(1 + N)$ over a load increment [100, 1000] with Eqs. (34) and (35), it is found that $1/\psi = 129.86$ and $\psi = 0.0077$; $1/\varepsilon_{vm}^{acc} = 29.925$

and $1/\varepsilon_{vm}^{acc} = 0.0332$. The same procedure has been used to compute eqs. (34) and (35) from the test data for isotropic stresses of 200 and 300 kPa. The values of ψ and ε_{vml}^{acc} for these three stresses are presented in Table 2. The fitted lines are shown in Fig. 5. In general, Eq. (33) fits the test data very well.

Examining the data in Table 2, it is found that both ε_{vml}^{acc} and ψ decrease with isotropic stress. The relationship of ε_{vml}^{acc} and ψ to the isotropic stress p_m scale is plotted in Fig. 6. It is seen from the figures that the data points are almost on a straight line. By best fitting these data points, it is found that:
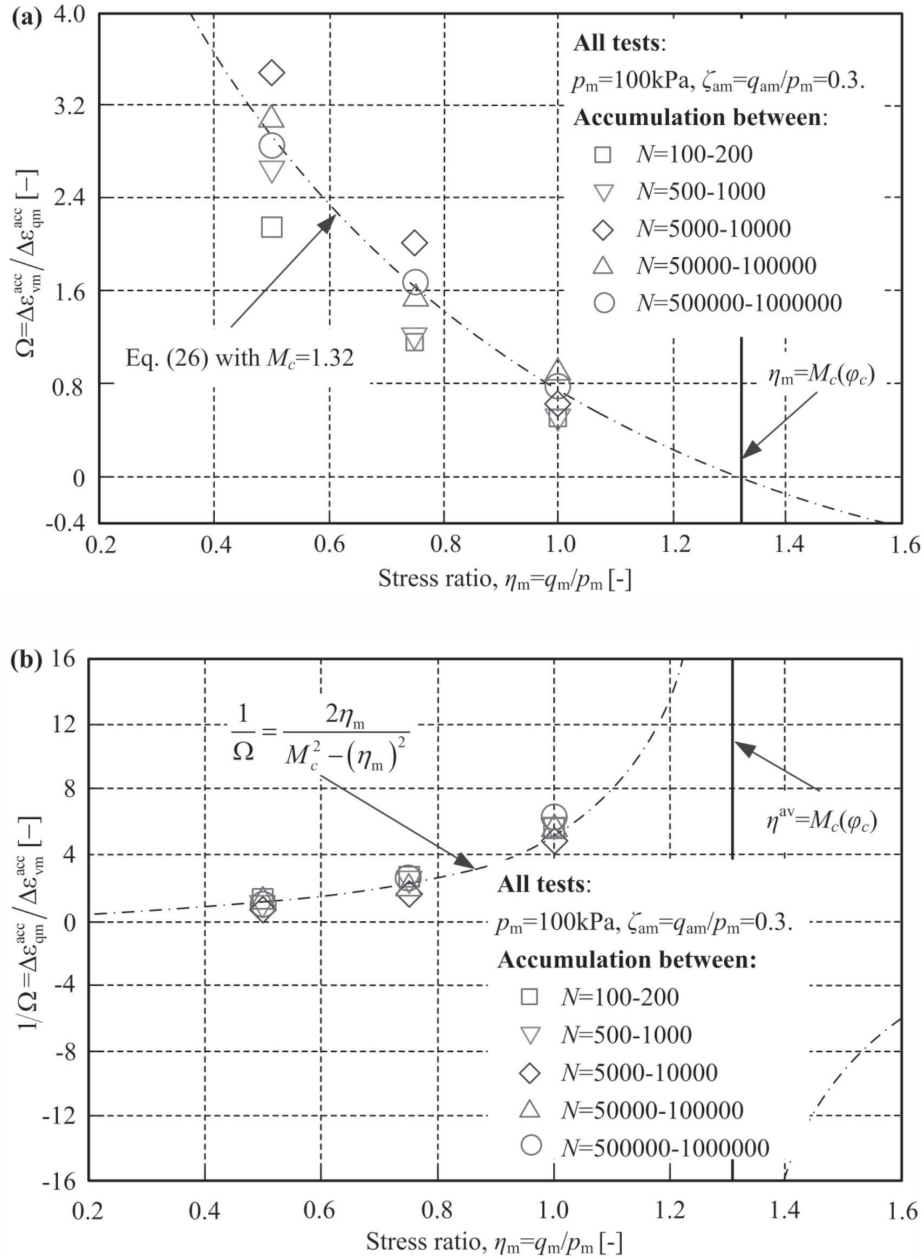
Fig. 8. Direction of strain accumulation as a function of the mean stress ratio from the flow rule of the modified Cam clay model is compared with the experimental results from cyclic triaxial tests in incremental form a) $\Omega = \Delta \varepsilon^{acc}_{vm}/\varepsilon^{acc}_{qm}$ and b) reciprocal value $1/\Omega$.

$$\varepsilon^{acc}_{vmlu} - \varepsilon^{acc}_{vml} = \varepsilon^{acc}_{vm,\,ref}\left(\frac{p_m}{p_{atm}}\right)^{\alpha} \tag{36}$$

and

$$\psi_u - \psi = \psi_{ref}\left(\frac{p_m}{p_{atm}}\right)^{\beta} \tag{37}$$

Where $\varepsilon^{acc}_{vmlu} = 0.0715$ and $\psi = 0.0065$ are in correspondence with $p_u = 1$ kPa (unit stress), p_{atm} is the standard atmospheric pressure, i.e., $p_{atm} = 100$ kPa. Fig. 6 (or Eqs. (36) and (37)) shows that the two

parameters ε^{acc}_{vml} and ψ are not constant, but decrease as the isotropic stress p_m increases with $\varepsilon^{acc}_{vml,\,ref} = 0.01$, $\alpha = 1$ and $\psi_{ref} = 0.001$, $\beta = 1$.

Simulation of Drained Cyclic Triaxial Compression Tests

With the values of K, ε^{acc}_{vml}, and ψ given by eqs. (32), (36) and (37), the proposed model has been fully calibrated for describing the accumulation of secondary deformation in granular soils under high-cyclic loading. Fig. 7 shows a comparison between experiments and corresponding predictions concerning the uniaxial accumulation of volume and deviatoric deformations

of sands subjected to different average stresses (p_m, q_m) = (100, 50), (100, 75), and (100, 100) kPa with a constant cyclic stress ratio ζ_{am} = 0.3. It was found that the numerical results match the experimental data well. Both permanent volumetric strain and deviatoric strain increase monotonically with the number of cycles, though predictions during the first load cycles appear to be somewhat inaccurate. However, this discrepancy is less important because the number of load cycles commonly associated with foundation deterioration lies far beyond one thousand.

Fig. 8 shows the direction of strain accumulation from the cyclic triaxial tests in incremental form $\Omega = \Delta\, \varepsilon^{acc}_{vm}/\varepsilon^{acc}_{qm}$. Both the measured directions of strain accumulation and the flow rule of the modified Cam-clay model are given in Fig. 8. It is seen that the flow rule of the modified Cam-clay model, i.e., a model for monotonic loading, approximates well the direction of strain accumulation under cyclic loading. That is to say, cyclic loading with average stress induces the accumulation of strain in the direction of average stress with the increase of the number of load cycles. The same conclusions as mentioned above were reported by Chang & Whitman [28].

Conclusions

Cyclic plasticity and cyclic viscoplasticity have been extensively studied for many years. However, classical constitutive models, such as the bounding surface models, are not suitable for accurately simulating the plastic deformation of soils under cyclic loading with a large number of cycles and relatively small loading amplitudes. In this study, a novel accumulation model for predicting the shakedown accumulation behavior of soils subjected to low-amplitude, high-cycle loading is proposed and validated. The following conclusions can be drawn from the study:

(1) Instead of using the conventional yield function in classical plastic theory, this paper proposes a phenomenological law to describe the shape of the compaction curve. The compaction curve is characterized by a logarithmic growth of the volumetric strain invariant as a function of the cycle number.

(2) Cyclic loadings with average stress result in the accumulation of strain in the direction of the average stress as the cycle number increases. This is implemented into the well-known modified Cam-clay model. The corresponding accumulated deviatoric strain is determined from the accumulated volumetric strain using the associated flow rule.

(3) The proposed model is calibrated by cyclic triaxial test results. The bulk modulus, K, used in the elastic stiffness $\mathbf{E}$ is determined by the rate of pore pressure accumulation in an undrained cyclic triaxial test and the rate of volumetric strain accumulation in a drained cyclic triaxial test $K = \dot{u}/\dot{\varepsilon}^{acc}_{vm}$. Accumulation model parameters ε^{acc}_{vml} and ψ are determined by

calculating the relationship of the normalized ratio $\ln (1+N)/\varepsilon^{acc}_{vml}$ to $\ln (1+N)$ from the measured data of volume strain accumulation against the number of cycles. Despite the small number of model parameters, the proposed model is able to achieve a satisfactory level of accuracy in its predictions.

Conflict of Interest

We declare that we have no financial and personal relationships with other people or organizations that can inappropriately influence our work, there is no professional or other personal interest of any nature or kind in any product, service and/or company that could be construed as influencing the position presented in, or the review of, the manuscript entitled "Modeling of accumulation of secondary deformation subjected to low-amplitude high-cycle loading in granular soils".

References

1. PAN K., XU T.T., LIAO D., YANG Z.X. Failure mechanisms of sand under asymmetrical cyclic loading conditions: experimental observation and constitutive modelling. Géotechnique, **72** (2), 162, **2022**.
2. LIU H., PISANÒ F., JOSTAD H.P., SIVASITHAMPARAM N. Impact of cyclic strain accumulation on the tilting behaviour of monopiles in sand: An assessment of the Miner's rule based on SANISAND-MS 3D FE modelling. Ocean Engineering, **250**, 110579, **2022**.
3. REEHANA S., MUTHUKUMAR M. Undrained response of fibre reinforced expansive soil subjected to cyclic loading. Soil Dynamics and Earthquake Engineering, **173**, 108154, **2023**.
4. CUI K., ZHANG D., LI Q., YANG S., ZHANG H. Experimental investigation on the accumulated strain of coarse-grained soil reinforced by geogrid under high-cycle cyclic loading. Geotextiles and Geomembranes, **51** (1), 233, **2023**.

ACCEPTED MANUSCRIPT

5. FUENTES W., MAŠÍN D., DUQUE J. Constitutive model for monotonic and cyclic loading on anisotropic clays. Géotechnique, **71** (8), 657, **2021**.

6. LI Y., NIE R., YUE Z., LENG W., GUO Y. Dynamic behaviors of fine-grained subgrade soil under single-stage and multi-stage intermittent cyclic loading: Permanent deformation and its prediction model. Soil Dynamics and Earthquake Engineering, **142**, 106548, **2021**.

7. SABERI M., ANNAN C.-D., KONRAD J.-M., LASHKARI A. A critical state two-surface plasticity model for gravelly soil-structure interfaces under monotonic and cyclic loading. Computers and Geotechnics, **80**, 71, **2016**.

8. MA B., ZHANG Q.-Q. A critical state three-dimensional multi-shear model for soil-structure interfaces under monotonic and cyclic loading. Engineering Structures, **295**, 116866, **2023**.

9. TAFILI M., DUQUE J., OCHMAŃSKI M., MAŠÍN D., WICHTMANN T. Numerical inspection of Miner's rule and drained cyclic preloading effects on fine-grained soils. Computers and Geotechnics, **156**, 105310, **2023**.

10. SUN Y., XIAO Y., HANIF K.F. Fractional order modelling of the cumulative deformation of granular soils under cyclic loading. Acta Mechanica Solida Sinica, **28** (6), 647, **2015**.

11. LI X., LIU J., NAN J. Prediction of dynamic pore water pressure for calcareous sand mixed with fine-grained soil under cyclic loading. Soil Dynamics and Earthquake Engineering, **157**, 107276, **2022**.

12. KHASAWNEH Y., BOBET A., FROSCH R. A simple soil model for low frequency cyclic loading. Computers and Geotechnics, **84**, 225, **2017**.

13. CHAI J.-C., MIURA N. Traffic-Load-Induced Permanent Deformation of Road on Soft Subsoil. Journal of Geotechnical and Geoenvironmental Engineering, **128** (11), 907, **2002**.

14. SAWICKI A., SWIDZINSKI W. Mechanics of a sandy subsoil subjected to cyclic loadings. International Journal for Numerical and Analytical Methods in Geomechanics, **13** (5), 511, **1989**.

15. SUIKER A.S.J., DE BORST R.A numerical model for the cyclic deterioration of railway tracks. International Journal for Numerical Methods in Engineering, **57** (4), 441, **2003**.

16. NIEMUNIS A., WICHTMANN T., TRIANTAFYLLIDIS T. A high-cycle accumulation model for sand. Computers and Geotechnics, **32** (4), 245, **2005**.

17. KARG C., FRANÇOIS S., HAEGEMAN W., DEGRANDE G. Elasto-plastic long-term behavior of granular soils: Modelling and experimental validation. Soil Dynamics and Earthquake Engineering, **30** (8), 635, **2010**.

18. JIA P.-F., KONG L.-W. Modeling of ratcheting accumulation of secondary deformation due to stress-controlled high-cyclic loading in granular soils. Journal of Central South University, **22** (6), 2306, **2015**.

19. CHEN W.B., FENG W.Q., YIN J.H., BORANA L., CHEN R.P. Characterization of permanent axial strain of granular materials subjected to cyclic loading based on shakedown theory. Construction And Building Materials, **198**, 751, **2019**.

20. ZHOU Z., MA W., LI G., SHEN M. A novel evaluation method for accumulative plastic deformation of granular materials subjected to cyclic loading: Taking frozen subgrade soil as an example. Cold Regions Science and Technology, **179**, **2020**.

21. WANG D., LIU E., ZHANG D., YUE P., WANG P., KANG J., YU Q. An elasto-plastic constitutive model for frozen soil subjected to cyclic loading. Cold Regions Science and Technology, **189**, 103341, **2021**.

22. LIAO D., YANG Z.X. Hypoplastic modeling of anisotropic sand behavior accounting for fabric evolution under monotonic and cyclic loading. Acta Geotechnica, **16** (7), 2003, **2021**.

23. ZHU Z., FU T., NING J., LI B. Mechanical behavior and constitutive model of frozen soil subjected to cyclic impact loading. International Journal of Impact Engineering, **177**, 104531, **2023**.

24. HE Z., WANG P., LIU Y. Cumulative deformation prediction and microstructure change of coarse-grained soil under cyclic loading. Soil Dynamics and Earthquake Engineering, **173**, 108136, **2023**.

25. CHEN G., LI P., LENG Z., WU T., LI C., XIANG J., LIU Y., HUO P. Transient model of unsteady creep of sliding zone soil under cyclic dynamic load based on fractional derivative. Alexandria Engineering Journal, **83**, 212, **2023**.

26. OLSZAK W., PERZYNA P. On thermal effects in viscoplasticity. Zeitschrift für angewandte Mathematik und Physik, **20** (5), 676, **1969**.

27. YIN J.-H. Non-linear creep of soils in oedometer tests. Géotechnique, **49** (5), 699, **1999**.

28. CHANG C.S., WHITMAN R.V. Drained Permanent Deformation of Sand Due to Cyclic Loading. Journal of Geotechnical Engineering, **114** (10), 1164, **1988**.